Powder Technology 487 (2027) 123416

Contents lists available at ScienceDirect

Powder Technology

journal homepage: www.journals.elsevier.com/powder-technology

Morphological evolution of granular geomaterials under impact erosion

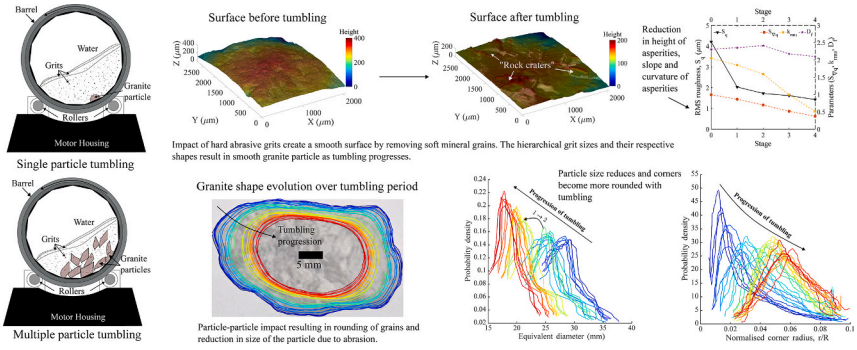
Emmanuel Okebunor Ashinze [a], Saurabh Singh [a,b,*], Matthew Richard Coop [a], Beatrice Anne Baudet [a]

[a] Department of Civil, Environmental and Geomatic Engineering, University College London, London, WC1E 6BT, UK
[b] School of Physics, Engineering, and Computer Science, University of Hertfordshire, Hatfield, AL10 9AB, UK

HIGHLIGHTS

- Independent controls on shape and texture of granite particle.
- Single particle tumbling – abrasive grit morphology drives texture evolution.
- Non-uniform distribution of mineral grains affects texture evolution.
- Initial shape dictates the shape of the particles after continued abrasion.
- Roughness is randomly distributed at various stages of multi-particle tumbling.

GRAPHICAL ABSTRACT



ARTICLE INFO

Keywords:
Shape modification
Rotary tumbling
Impact abrasion
Surface texture
Roughness
Power spectral density

ABSTRACT

This study investigates the evolution of surface roughness and particle shape, two parameters that define the structure and mechanical behaviour of geomaterials, and shows that both can be controlled by tumbling. Two tumbling approaches were employed to study the evolution of the shape and texture of granite particles. Single-particle tumbling with abrasive grit was used to examine the controlled evolution of surface roughness, while multiparticle tumbling, with and without abrasive powder grits, was used to analyse the evolution of particle shape. The size and shape of the powder grits were characterised using optical microscopy with the Morphologi G3 system. A mechanism was hypothesised for different stages of single-particle tumbling and validated against the experimental evidence. Specifically, the large, elongated and angular grit particles used in the initial stages, which are harder than granite or any other natural geomaterial, alter the low-frequency features of the surface topography, whereas the small circular and rounded grits suppress the high-frequency features of the surface, i.e. the roughness. Additionally, multiparticle tumbling was carried out to study shape and texture evolution with time. The surface and shape of the granite ballast particles were characterised at different stages of tumbling using optical/specular reflectance, root-mean-square roughness, Fourier amplitude spectra or power spectral density, and peak-count distribution, in addition to roundness, circularity, and size distribution for multiparticle tumbling. This research highlights that tumbling a single rock particle with different grits produces a controlled

* Corresponding author at: School of Physics, Engineering, and Computer Science, University of Hertfordshire, Hatfield, AL10 9AB, UK
E-mail addresses: emmanuel.ashinze.24@ucl.ac.uk (E.O. Ashinze), s.singh29@herts.ac.uk (S. Singh), m.coop@ucl.ac.uk (M.R. Coop), b.baudet@ucl.ac.uk (B.A. Baudet).

https://doi.org/10.1016/j.powtec.2026.123416
Received 30 July 2026; Received in revised form 10 October 2026; Accepted 22 October 2026
Available online 24 October 2026
0032-5910/© 2026 The Authors. Published by Elsevier B.V. This is an open access article under the CC BY license (http://creativecommons.org/licenses/by/4.0/).

evolution of roughness, whereas multiparticle tumbling results in a controlled shape evolution with randomly varying texture.

Notation

α	slope of the linear part of the power spectral density
δ	current dimension value
δ_o	initial dimension value
k_{rms}	root-mean-square curvature
A_c	area of the equivalent circle
A_p	area of the particle
$C_r(q)$	radially averaged power spectral density
C_x	convexity
D_f	fractal dimension
I	dimension of the intermediate particle axis
L	dimension of the longest particle axis
P	perimeter of the particle
P_{cx}	perimeter of the convex hull
q_x, q_y	spatial frequencies (wavenumbers)
r	average radius of the corner circles
r_i	radius of the i^{th} corner circle
R	radius of the largest inscribed circle
S	current value of shape descriptor(s)
S_o	initial value of shape descriptor(s)
$\frac{S-S_o}{1-S_o}$	relative shape descriptor(s)
$S_{\nabla q}$	root-mean-square slope
S_q	root-mean-square roughness

1. Introduction

Geomaterials are studied in both earth sciences and civil engineering. Under a diverse combination of physical, chemical, and biological weathering processes, together with erosion and transportation over long periods, rock degrades into silt, sand, and gravel, each with characteristic shape and size distributions [1–5]. These characteristic shape and size distributions also evolve during handling or maintenance (such as rockfill handling and ballast tamping) and during hazardous flows (landslides or debris flows) via impact abrasion and wear [6–8]. It is well established that the shape and size parameters affect the mechanical behaviour of granular deposits through interactions at the contacts and through the particle arrangement, or fabric [9–14]. The mechanics of solids at the contact are well understood for regularly shaped, smooth, elastic particles, for which models such as that of Hertz [15] can be used; however, divergence from these requires other parameters to be considered. One common factor that influences the contact behaviour is surface roughness, for which dedicated contact laws have been developed [16–18]. The effect of particle shape, on the other hand, will affect particles' interlocking and the overall shearing resistance, and it is now more common to simulate the irregular shapes in the discrete element models of soils [19,20]. Separating the effects of shape and roughness on the mechanical behaviour at the micro- and macroscales is not straightforward. This study therefore investigates the evolution of characteristic size and shape distributions of granular geomaterials subjected to rotary mill tumbling, with the aim of creating particles with controlled shape and/or roughness.

Previous researchers have applied a systematic control over the size and shape of granular materials in order to study their effects on the sample- and particle-scale behaviour [12,21,22]. Typical methods of achieving this control are sieving or filtering, acid etching, crushing, milling, and abrasion [10,23,24], the last of which is commonly used for rock and ballast particles [25]. Early studies of the controlled abrasion of gravel-sized particles used tumbling barrels to explore the effect of repeated impacts of silt on particle shape [26–28]. The particles, of similar hardness, are continuously lifted and dropped, and collide with one another, as the tumbler rotates. This repeated motion primarily abrades particles by removing surface asperities and sharp edges, producing extensive shape evolution through attrition, chipping, and rounding [29]. The effects of tumbling on particle shape and size have been widely studied because of their significant influence on particle form, including roundness and sphericity [27,28]. Recent studies also utilise three-dimensional imaging techniques such as X-ray Computed Tomography [30], close-range photogrammetry [31], and 3-D laser scanning [32] with resolutions on the order of hundreds of microns to study the particle shape evolution (form, corner radius or roundness, and fractal dimension) in the Micro-Deval test. However, the resolution of these imaging techniques was not sufficient to quantify the evolution of roughness.

In order to include roughness as well as shape in the parameters controlled by tumbling, a careful choice of abraded and abrading material needs to be made. Here, crushed granite (ballast) provided the parent material and was used as both the abraded and the abrading material. The use of different types of hard abrasive grit allowed both the shape and the surface texture to be controlled. Based on the size, shape, and hardness of the grit particles, weathering mechanisms were hypothesised for the different stages of tumbling. The evolution of the surface characteristics was analysed in the light of the proposed hypothesis. In tests during which only crushed rock particles were tumbled, the evolution of particle size, shape and texture was studied.

2. Materials and experimental methods

A comprehensive study was conducted of the evolution of the texture and shape of granite ballast through single-particle tumbling in the presence of hard abrasive powder grit, and multiparticle tumbling performed both with and without powder grit. In rotary tumbling involving several particles, textural modifications are accompanied by changes in particle size and shape, while surface roughness varies sporadically. Single-particle tumbling was therefore performed to isolate surface roughness evolution from changes in particle size and shape.

2.1. Materials

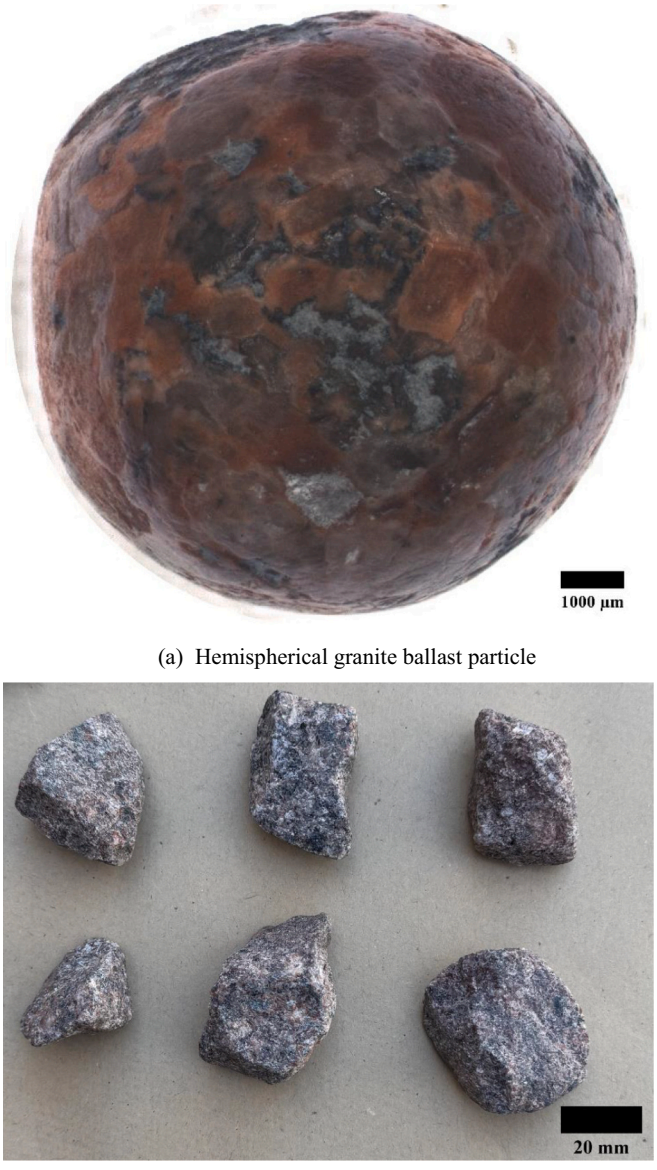
A UK granite ballast of granodiorite origin, sourced from Mountsorrel Quarry in Leicestershire, England, was used as the parent material to study the evolution of surface texture and shape in rotary mill tumbling. The granite ballast particles are primarily composed of quartz, plagioclase, potassium feldspar, amphibole, and biotite (mica), with an average Vickers hardness of 6.39 GPa [33], a specific gravity of 2.65

Table 1
Mechanical properties of Mountsorrel granite (Afrouz, 1992).

Material	Relative density	Compressive strength (MPa)	Poisson's ratio	Young's modulus (GPa)	Shore (Vickers') hardness
Granite	2.65	176.40	0.25	60.60	77.0 (6.39 GPa)

[34], and a Poisson's ratio of 0.25 [35]. Table 1 lists the key mechanical properties of the Mountsorrel granite.

Four types of grit were used at different stages of the tests: coarse, medium-sized, pre-polish, and polish grit. The coarse, medium-sized, and pre-polish grits are made of silicon carbide (SiC), and the polish grit is made of aluminium oxide (Al_2O_3), with Vickers hardness values of 24 to 32 GPa and 18 to 28 GPa [36,37], respectively. Two types of tumbling experiments were performed: single-particle tumbling with abrasive grit and multiparticle tumbling with and without abrasive grit. Single-particle tumbling (controlled tumbling) was carried out to study the evolution of the surface texture of regularly shaped particles, while multiparticle tumbling was performed to assess combined textural and morphological changes in naturally irregular crushed rock. For single-particle tumbling, four granite ballast particles were machined into 12 mm diameter spheres and then cut into hemispheres (Fig. 1a). The hemispherical shape was chosen to ensure that the same apex region of the particle was scanned each time. In multiparticle tumbling, irregular granite ballast particles (crushed rock) ranging from 23 to 40 mm in size were used as obtained from the quarry (Fig. 1b). Sixty fresh UK granite particles were selected and divided equally between the two conditions: with-grit tumbling and without-grit tumbling. This number was chosen on the basis of previous morphological studies in which twenty randomly selected particles were used for surface roughness characterisation [38]; therefore, a minimum of twenty particles was considered sufficient for morphological analysis. The particles were washed, oven-dried, and each was labelled at its stable resting point, which was identified from repeated free-fall tests.



(a) Hemispherical granite ballast particle

(b) Irregular granite ballast particles

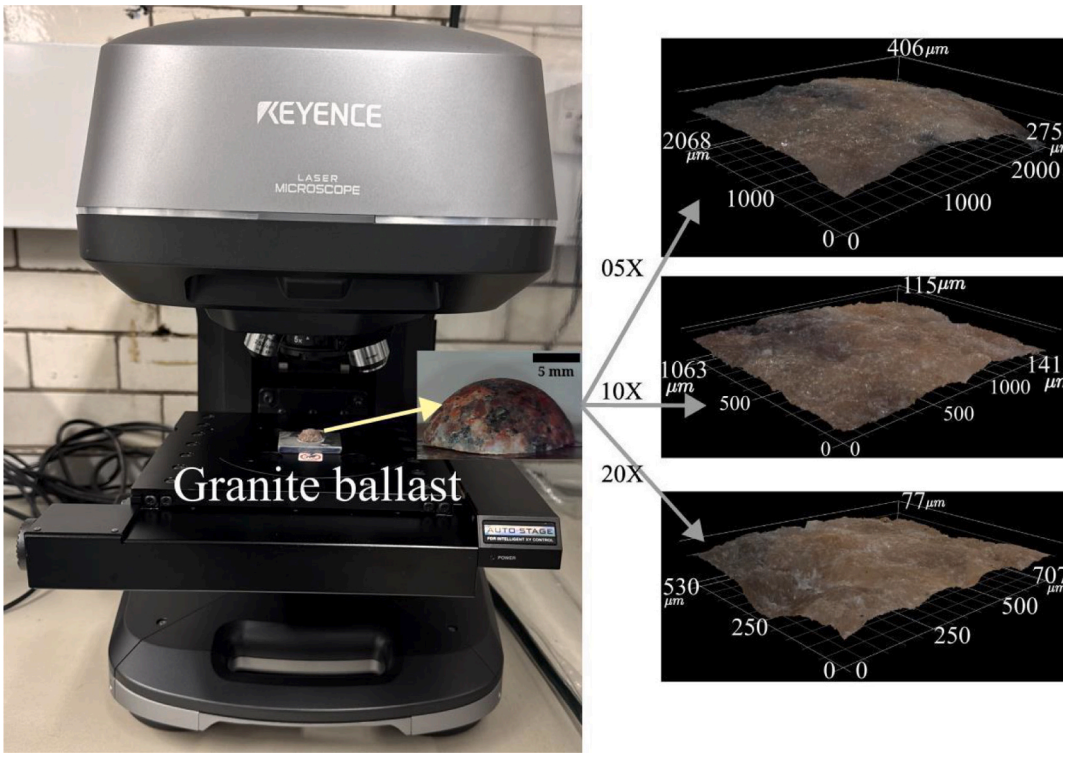
Fig. 1. Images of example granite ballast particles used in this study: (a) Hemispherical granite ballast particle, (b) Irregular granite ballast particles.

2.2. Shape and surface texture analysis

The size and shape of the grits were determined using a Malvern Morphologi G3 microscope, whereas for the crushed granite, which was too large for the microscope, high-quality images were captured using a digital camera (see Section S.0 of the Supplementary document). A Keyence laser confocal microscope was used to scan the surface of the granite particles. Both optical images and height maps were obtained with 5× (spatial resolution: 2.69 µm, vertical resolution: 0.1 nm), 10× (spatial resolution: 1.38 µm, vertical resolution: 0.1 nm), and 20× (spatial resolution: 0.69 µm, vertical resolution: 0.1 nm) objective lenses to track the evolution of the surface texture. To ensure that the scans were performed at the same location on each particle, the particle was centred on a rotational stage and manually oriented to match the previous 5× scan. The procedure was repeated at 10×, after which the lens was switched to 20×, and the scan was performed. This scan was compared directly with the previous 20× scan using the Keyence analysis software (VK-X 3000 MultiFileAnalyzer), which provides the rotation required to correct the orientation. Fig. 2a shows the Keyence microscope scanning the hemispherical granite particle, along with the 3D optical images generated from scanning the peak of the particle for different objective lenses. The initial surface roughness (S_q) of the hemispherical and irregular granite particles was 4.1 µm and 3.3 ± 1.1 µm, respectively.

Tumbling of a single hemispherical particle was performed using a rock tumbler (Fig. 2b), with a barrel of 103 mm outer diameter, 92 mm inner diameter, and 80 mm height, in the presence of water and abrasive grit, at 150 rpm. The Morphologi G3 was also used to characterise the shape of grits and residue from tumbling. Single-particle tumbling was carried out in four stages using 10 g of coarse, medium-sized, pre-polish, and polish grit, respectively. The size and shape descriptors of these powder grits were obtained using the Malvern Morphologi G3 and are described in the next section. Each stage involved daily tumbling for seven days, followed by washing and oven-drying of the particles. Interrupted scans were performed at 24-h intervals to characterise the texture. Prior to each scan, the particles were washed with running water and oven-dried for 30 min.

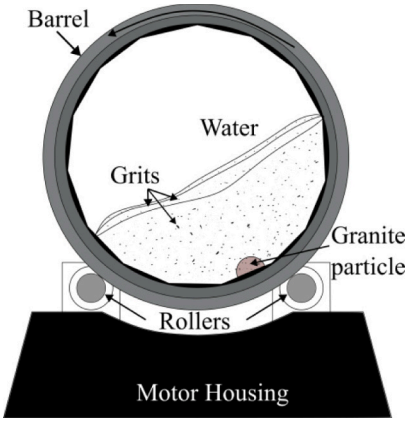
For multiparticle tumbling with grit, 100 g of powder grit was used at each stage, based on the concentration of 1 g per 10 L of water adopted in the single-particle tumbling experiment. Interrupted scanning and data acquisition were carried out after cumulative tumbling times of 0 min, 10 min, 20 min, 30 min, 1 h, 2 h, 4 h, 8 h, 16 h, and 24 h, and then daily for five days for each tumbling stage (20 days in total), with the same procedure applied to tests without grit. For each scan and data acquisition, the particles were washed, oven-dried for 30 min, and weighed to determine total and individual particle weights. High-quality images of the particles positioned in their stable configuration were taken for shape analysis, and particle heights were measured with a digital calliper. Five particles from each of the with-grit and without-grit experiments were scanned using a Keyence laser microscope, at approximately the same surface location, to quantify surface roughness. The fines generated by abrasion during multiparticle tumbling were collected and subjected to morphological analysis. The collected fines were scanned up to three times to confirm the consistency of the results.



(a) Laser confocal microscopy and granite ballast



(b) Rock tumbler



(c) Sketch of the internal mechanism

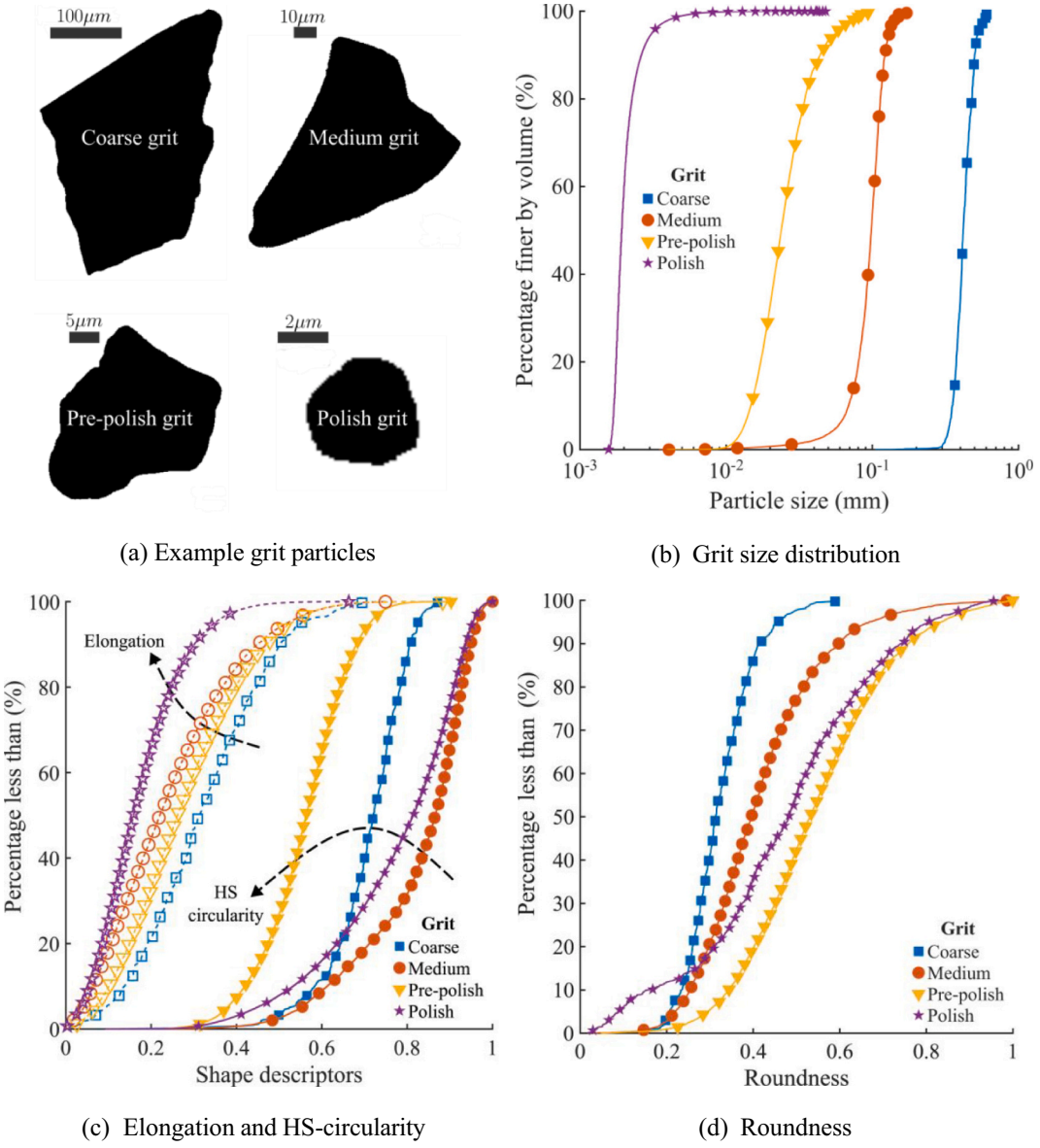
Fig. 2. Laser confocal microscopy and Rock Tumbler: (a) Laser confocal microscopy and granite ballast, (b) Rock tumbler, (c) Sketch of the internal mechanism.

3. Morphology of grits and tumbling mechanism

The choice of powder grit is typically determined by size, while other characteristics, such as its morphology, are usually overlooked. The hypothesis here was that the morphology of the powder grit influences the gradual change in surface texture and shape of the tumbled particles. The shape of the grit was analysed using the Malvern Morphologi G3 microscope at different magnifications. Fig. 3a shows scanned images of single grit particles: the coarse grit tends to be highly elongated and very angular, while the medium-sized grit is similarly elongated but slightly less angular. The pre-polish and polish grits are more rounded than the coarse and medium-sized grits. The particle size distributions of the different types of grit are shown in Fig. 3b, with the circle-equivalent (CE) diameter taken as the particle size.

Three useful shape descriptors were chosen to best describe and distinguish between the different types of grit: elongation, which measures the length of a particle relative to its width; high-sensitivity (HS) circularity, which measures how closely the shape approaches a circle; and roundness, which gives a measure of angularity. The definitions of the three shape descriptors are given in Table 2, where the range and median values of grit sizes and shape parameters are summarised. All descriptors were computed by the software built into the Morphologi G3 apparatus, except for roundness, which was computed from microscope images of individual grit particles using MATLAB [39]. The cumulative frequency curves in Fig. 3c show that the coarse and medium-sized grits contain more elongated particles than the pre-polish and polish grits, while HS circularity curves indicate that the coarse grit is more irregular than the pre-polish and polish grits. The medium-sized grit shows a higher proportion of particles with HS circularity values tending towards 1. The roundness values plotted in Fig. 3d indicate that the coarse grit tends to be sub-angular, the medium-sized grit sub-rounded, and the pre-polish and polish grits generally well rounded.

In single-particle tumbling, individual grit particles interact with the granite surface in the rotary mill. A hypothesised mechanism for this



(a) Example grit particles (b) Grit size distribution

(c) Elongation and HS-circularity (d) Roundness

Fig. 3. Size and shape characteristics of powder grits using the Morphologi G3 apparatus: (a) Example grit particles, (b) Grit size distribution, (c) Elongation and HS-circularity, (d) Roundness.

Table 2
Shape descriptors and their values, range (median), for powder grits.

Size and shape descriptors	Coarse grit	Medium grit	Pre-polish grit	Polish grit
Diameter, mm	0.30–0.60 (0.42)	0.04–0.18 (0.10)	0.015–0.08 (0.024)	0.002–0.048 (0.002)
Roundness $\left(\frac{\sum_{i=1}^{n} r_i/R}{n}\right)$	0.20–0.40 (0.31)	0.23–0.58 (0.40)	0.24–0.72 (0.53)	0.28–0.78 (0.48)
Elongation (I/L)	0.04–0.40 (0.31)	0.04–0.52 (0.22)	0.046–0.48 (0.26)	0.12–0.54 (0.16)
HS circularity $(4\pi A/P^2)$	0.44–0.80 (0.72)	0.48–0.96 (0.87)	0.36–0.72 (0.56)	0.44–1.00 (0.81)

interaction is presented in Fig. 4. As the granite minerals are significantly softer than the SiC and Al_2O_3 components of the grit, the interaction results in the removal of asperities. It is hypothesised that in the first stage, elongated and angular grit particles, whose median size is 420 μm (i.e. equivalent to several asperities), collide with the granite

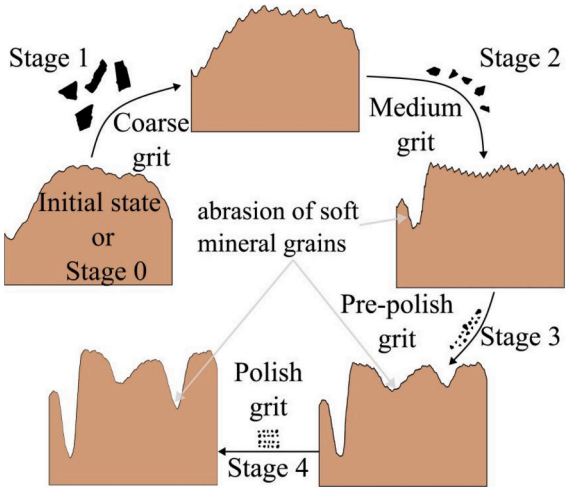


Fig. 4. Hypothesis for the mechanism of single particle tumbling.

particle surface and remove or suppress soft chunks of asperities, leaving large impressions. The surface of geomaterials is often described as fractal, meaning that its shape can be represented as a superposition of waves of different frequencies [18,40,41]. The action of the coarse grit would affect only the low-frequency features of the fractal surface of the granite particle, akin to the "corners" of the particle, due to its comparatively large size (Fig. 4). In the second stage, the medium-sized grit particles, which have a higher number density per unit surface area of the granite particle because of their smaller size (100 μm), would impact the surface significantly more often over the same duration of tumbling. The action of the medium-sized grit would affect the low- to medium-frequency features because of its size, resulting in a reduction in roughness amplitude but an increase in asperity density. In the third stage, the number density of the pre-polish grit, which is almost 8000 times that of the coarse grit, would result in significantly more impacts than in the previous stages. The size of the pre-polish grit particles (24 μm), now commensurate with that of some asperities, means that they would act on both low- and high-frequency features. This would result in an overall suppression of both roughness amplitude and asperity density. In the final stage, the polish grit particles, which are the finest (2 μm) and are smaller than the roughness of natural granite ballast, would, by repeated impact, suppress the roughness further. The tumbling results presented below are analysed in the light of this hypothesis.

The analyses in Section 4 are performed to validate the above hypothesis, where the surface condition at each tumbling stage results from the abrasion accumulated over all preceding stages. The results therefore reflect the cumulative effect of progressive abrasion from tumbling with grits of different sizes of SiC and Al_2O_3.

4. Evolution of particle morphology at the scale of surface roughness: single-particle tumbling

Each hemispherical particle was subjected to the four stages of abrasion using different grades of powder grit. Optical images of the surface revealed visible alterations. Between the initial state (Fig. 5a)

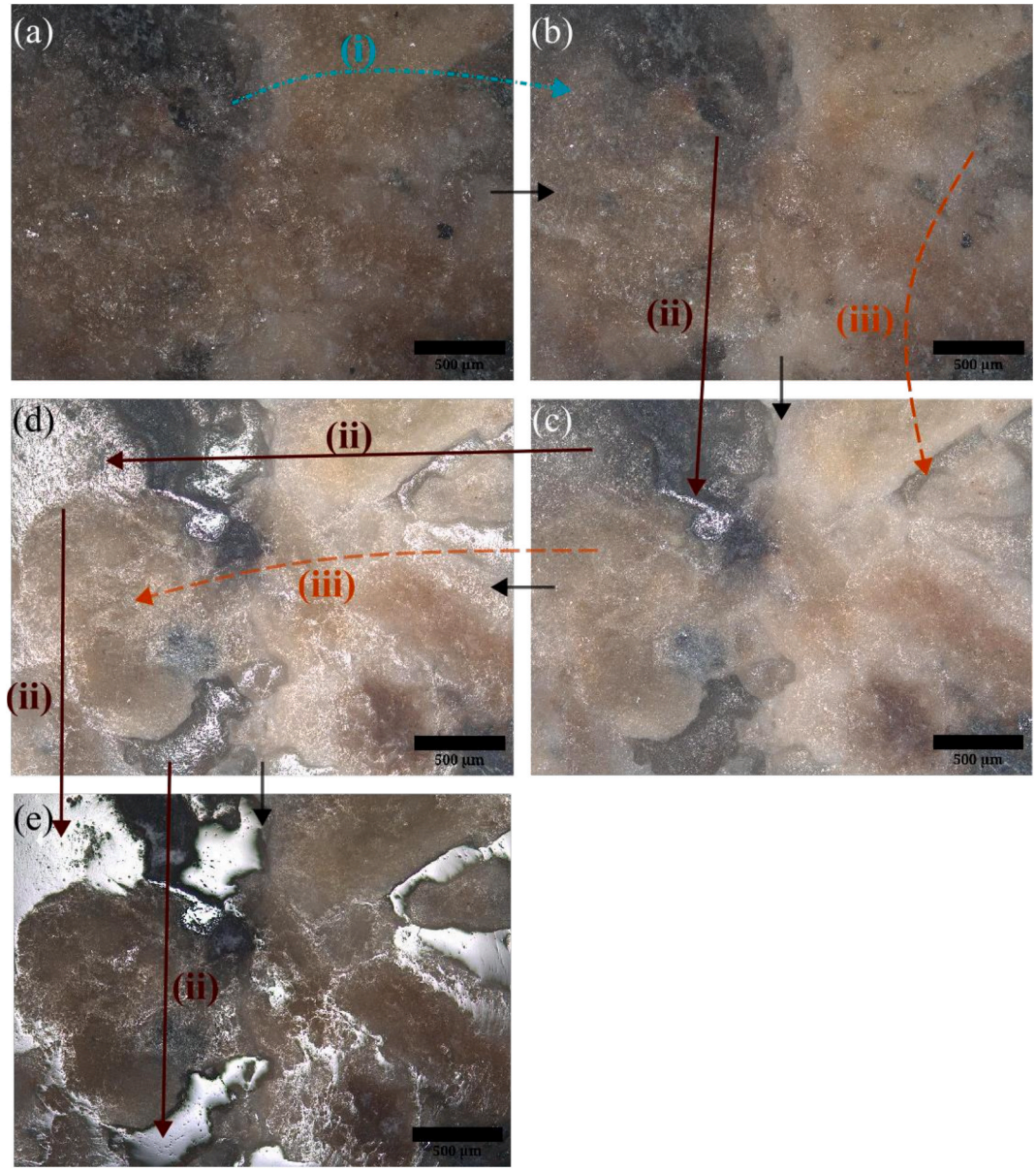


Fig. 5. Evolution of optical reflectance and surface appearance in single-particle tumbling: (a), (b), (c), (d), (e) denote different stages of tumbling ([i]surface brightening, [ii]Polishing of quartz, [iii]Removal of softer minerals).

and the end of stage 1 with coarse grit (Fig. 5b), the high hardness of the grit resulted in strong abrasive action on the particle, causing the darker mineral regions containing biotite (mica) to be abraded first due to their low hardness of 1.5 GPa [42]. This led to the progressive removal of surface layers and a lighter appearance. During stage 2 with medium-sized grit, surface depressions resembling "rock craters" formed (Fig. 5c); these had not developed with the coarse grit alone, even after extended tumbling. The depressions became more pronounced during stage 3 with pre-polish grit, as seen from the lighter surrounding areas (Fig. 5d), owing to the rounded shape of the grit, although the surface was not yet glassy. Finally, stage 4 with fine polish grit produced a reflective, glassy surface (Fig. 5e). The polish grit removed only minute amounts of material, leaving the particle smooth, in contrast to the rough surface created by the large, elongated coarse grit.

Changes to the surface of the granite particle were also clearly reflected in the surface height maps and cross-sectional profiles. Fig. 6 shows the surface height maps at the end of each tumbling stage. A distinct set of topographical features, referred to as "rock craters", appears from stage 2 and becomes more prominent by the end of stage 4. These features should correspond to relatively hard mineral grains, as soft ones abrade away in tumbling. The height-map texture also becomes smoother across the tumbling stages. Fig. 6e and f show the cross-sectional profiles along the x- and y-axes passing through the peak of the initial surface. These surfaces were referenced at a particular region to show the differences in height (Fig. 6e); however, these differences are not real, since the reference region itself abrades during tumbling. The profile at stage 0 represents the particle before tumbling; the profile height decreases as the tumbling stages advance. The coarse and

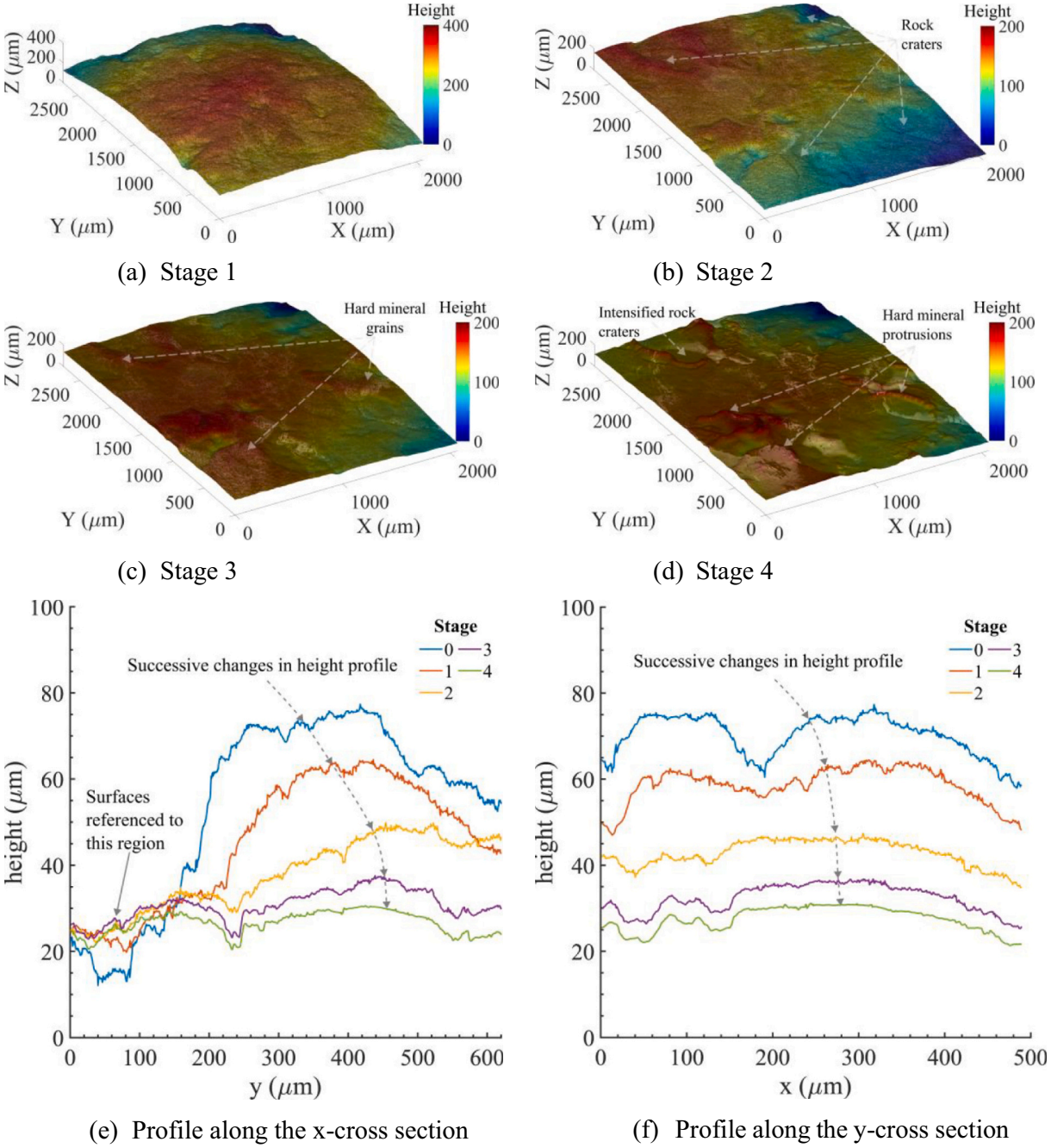


Fig. 6. Evolution of surface through 3d height maps and profiles in single-particle tumbling: (a) Stage 1, (b) Stage 2, (c) Stage 3, (d) Stage 4, (e) Profile along the x-cross section, (f) Profile along the y-cross section.

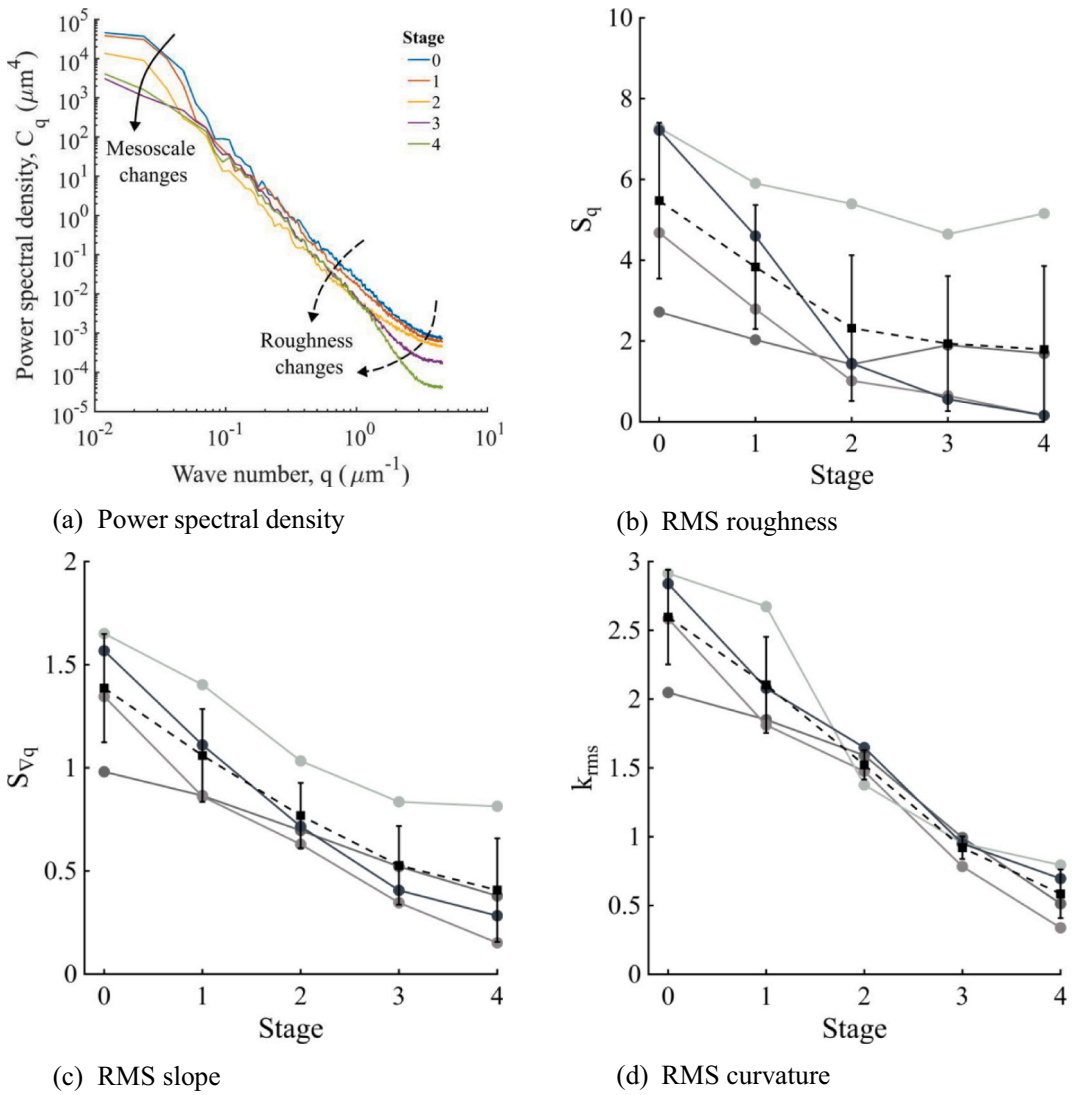


Fig. 7. Evolution of power spectral density and PSD parameters in single-particle tumbling: (a) Power spectral density with tumbling stages, (b) Root-mean-square roughness, (c) Root-mean-square slope, (d) Root-mean-square curvature. Error bars represent the 95% confidence interval of the mean ($n = 4$ particles).

medium-sized grits produce the largest reductions in the height profile, consistent with the hypothesis stated earlier. From stage 0 to stage 1, the roughness amplitude appears to decrease; however, the asperity density increases. Similar results are seen for the medium-sized grit from stage 1 to stage 2. The pre-polish and polish grits reduce both asperity density and roughness amplitude, as seen from the profiles at the end of stages 3 and 4.

Yang et al. [41] showed how power spectral density (PSD) analysis, as introduced by Nayak [40], can be applied to the surface heights of geomaterials, since these result from random weathering processes. This way of analysing the profilometry data provides a more objective measurement of the roughness than the microscope's built-in motif method, in which the roughness is separated from the waviness of the surface by a function that may not capture the irregular surface of the geomaterials. Other researchers [43] have shown that the motif method is scale-dependent, which can affect the roughness measurements. The PSD method was therefore adopted, and the height maps of the surfaces produced at each tumbling stage, $h(x,y)$, were analysed using the Fourier transform of the autocorrelation function [40]:

$$C\left(q_x, q_y\right) = \frac{1}{(2\pi)^2}\iint_{-\infty}^{\infty}\left\{\lim_{\substack{L_1\to\infty \\ L_2\to\infty}} \frac{1}{4L_1L_2}\int_{-L_1}^{L_1}\int_{-L_2}^{L_2} h(x_0,y_0)h(x+x_0,y+y_0)dx_0dy_0\right\} exp\left[-i\left(xq_x+yq_y\right)\right]dxdy \quad (1)$$

where q_x and q_y are the spatial frequencies (wavenumbers).

Because of the random nature of the tumbling process, the surface

roughness was assumed to be isotropic, and a radially averaged power spectral density ($C_r(q)$) with spatial frequency ($q = \sqrt{q_x^2 + q_y^2}$) was calculated using the algorithm proposed by Persson et al. [44] and plotted in Fig. 7 along with the parameters obtained using the PSD. The linear part of the PSD is associated with a self-affine surface, i.e. a self-similar surface with different fractal qualities in the directions tangential and normal to the surface [41]. Parameters such as the root-mean-square roughness (S_q), root-mean-square slope ($S_{\nabla q}$), and root-mean-square curvature (k_{rms}) of the rough surface can be estimated from the PSD using the following equations:

$$S_q = \sqrt{2\pi \int q C_r(q) dq} \tag{2}$$

$$S_{\nabla q} = \sqrt{2\pi \int q^3 C_r(q) dq} \tag{3}$$

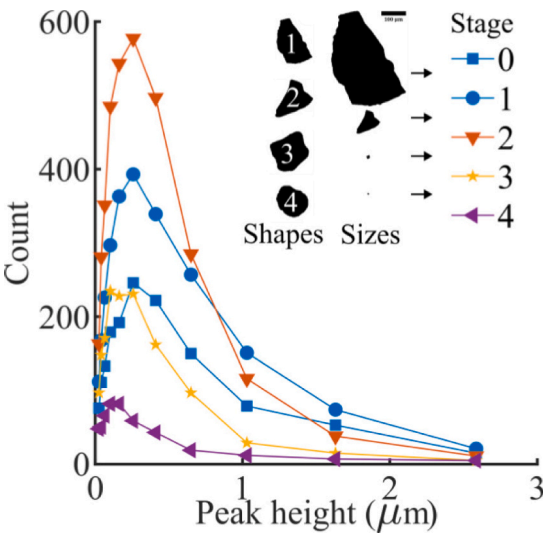
$$k_{rms} = \sqrt{2\pi \int q^5 C_r(q) dq} \tag{4}$$

The value of S_q corresponds to the root-mean-square value usually determined by the motif method after removing the form or waviness from the surface, and therefore represents the true roughness. The fractal dimension D_f can also be calculated from the slope (α) of the linear part of the PSD using

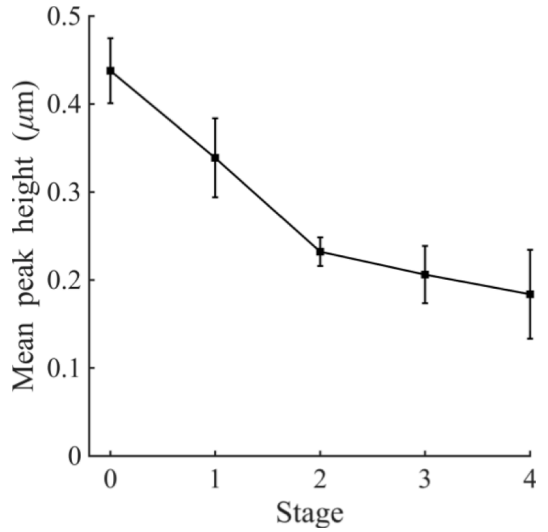
$$D_f = 4 + \alpha/2 \tag{5}$$

For the power spectral density (PSD) analysis, height maps of 415 × 415 μm (600 × 600 pixels) spatial dimensions with a spatial resolution of 0.691 μm and a vertical resolution of 0.1 nm were used. The PSD was computed using Persson et al.'s [44] algorithm, and corresponding parameters were calculated over a spatial-frequency (wavenumber) range of 0.02 to 2.50 μm^{-1}. The results of the power spectral density analysis are presented in Fig. 7. As shown in Fig. 7a, the initial stages of tumbling primarily affect the roundness or mesoscale shape features (corresponding to low frequencies), whereas the pre-polish and polish grits suppress the high-frequency features, leaving the mesoscale features nearly unaffected. Fig. 7b, c, and d present the parameters obtained from the PSD, namely S_q, $S_{\nabla q}$, and k_{rms} (D_f is presented in the supplementary) for data obtained from single-particle tumbling tests performed on four different hemispherical granite particles. The asperities become smaller and flatter as S_q, $S_{\nabla q}$, and k_{rms} all decrease over the tumbling stages. The rms roughness, S_q, has some scatter due to differences in initial values; however, the trend suggests an overall decline in roughness with stages.

Counting the asperity peaks and their heights allows the evolution of the particle surface to be tracked across successive tumbling stages (Fig. 8a). At low heights (0–1 μm), the peak count increased from stage 0 to stage 2 and then decreased from stage 2 to stage 4, whereas the count of higher peaks (greater than 1.4 μm) increased only from stage 0 to stage 1, followed by a steady decline. This suggests that the coarse and medium-sized grits remove the larger peaks but, because of their elongated shape, create new, smaller peaks, whereas smaller, rounded pre-polish and polish grits in later stages flatten the surface without generating new peaks. The mean peak height, averaged for each stage from four tests, was also computed across the tumbling stages, showing a consistent decrease as the process progressed (Fig. 8b). Understanding these patterns for different minerals could allow the shape and roughness of particles, tested in microscale experiments, to be controlled, and the suitability of existing contact models for geomaterials to be explored more fully.



(a) Peak height distribution with tumbling stages



(b) Average peak height with tumbling stages

Fig. 8. Distribution of peak height and mean surface height through tumbling stages in single-particle tumbling: (a) Peak height distribution with tumbling stages, (b) Average peak height with tumbling stages. Error bars represent the 95% confidence interval of the mean ($n = 4$ particles).

5. Evolution of particle morphology at the scale of particle size and shape: multiparticle tumbling

A separate issue is to understand how weathering occurs in nature, and here it is investigated by carrying out tumbling of multiple irregular granite particles, which then undergo a range of morphological changes due to asperity removal [45], splitting, crushing, chipping, cracking, and grinding [28]. These morphological changes are quantified through weight loss, changes in particle size, and variations in shape descriptors. As in single-particle tumbling, the evolution of surface roughness is also investigated. Fig. 9 shows the progressive change in particle boundaries with increasing tumbling time. It is evident that the most rapid changes

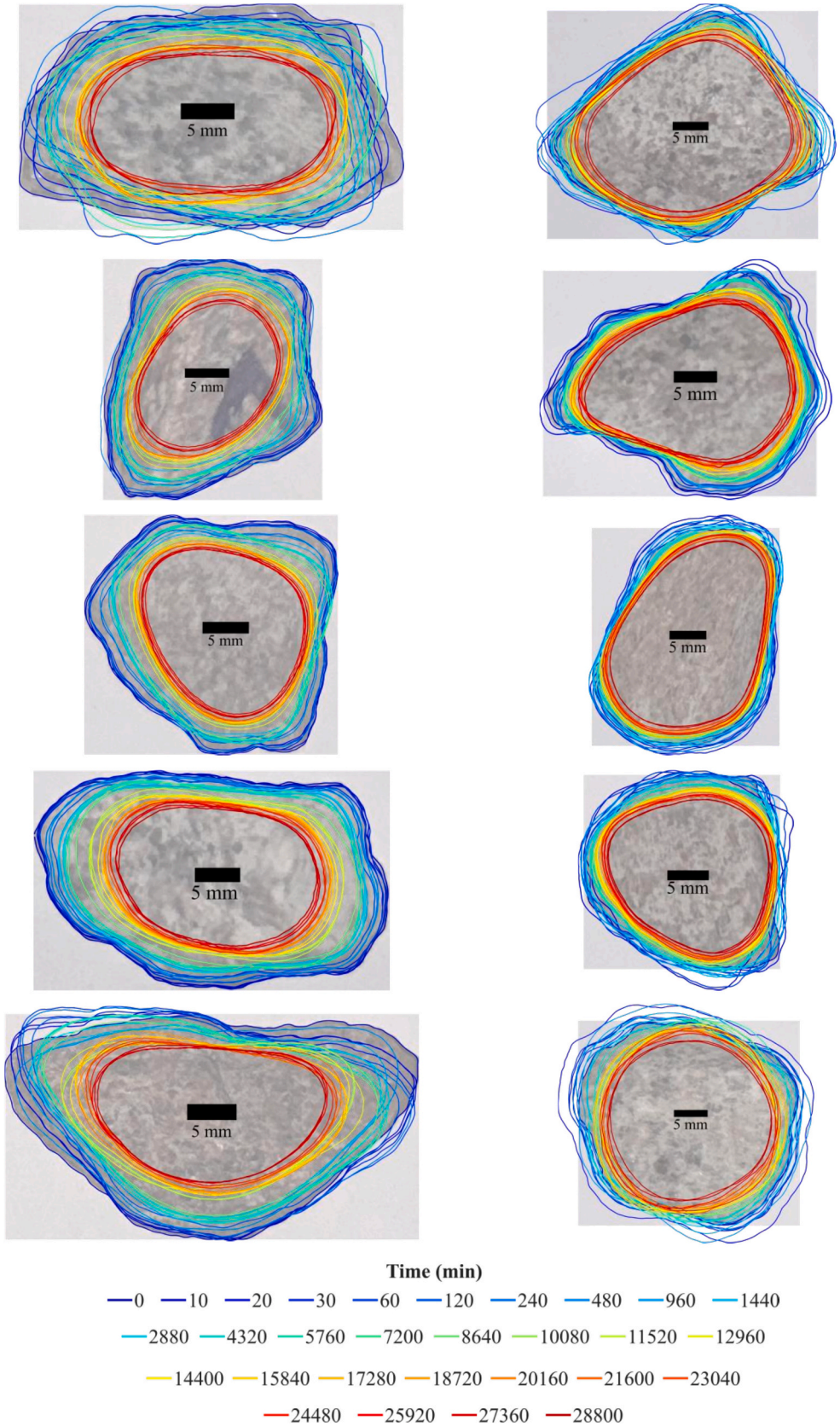


Fig. 9. Evolution of particle shape (boundary) with time in multiparticle tumbling.

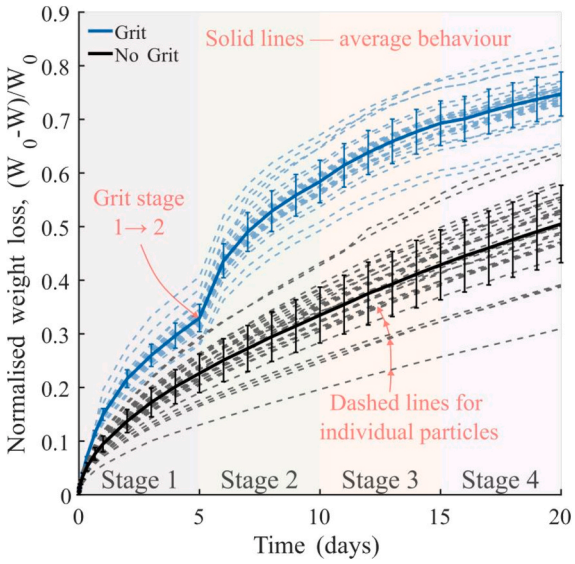


Fig. 10. The relationship between weight loss and tumbling time in multi-particle tumbling. Error bars denote ±1 standard deviation ($n = 30$ particles).

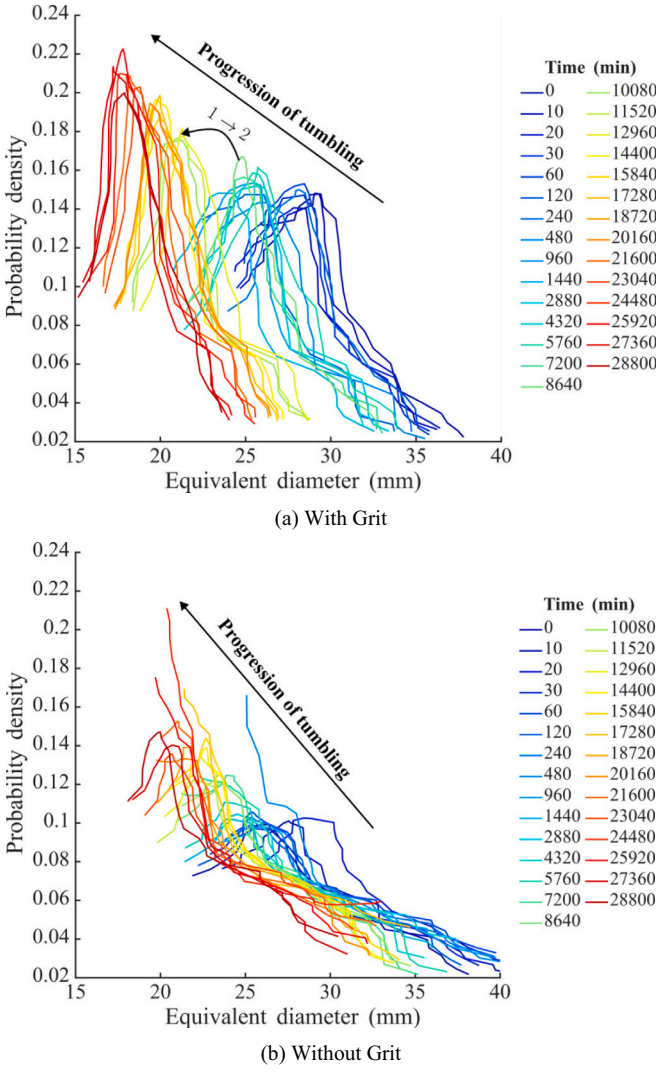


Fig. 11. Evolution of equivalent diameter (particle size) with progressive multiparticle tumbling: (a) With grit, (b) Without grit.

occur during the early stages of tumbling, as illustrated by the transition from the blue to the cyan boundaries within the first day. Material loss seems greatest at sharp, angular corners, while rounded corners exhibit slower changes in outline. This indicates that non-convex and angular regions abrade faster than convex and rounded regions. The evolution of particle boundaries not only reflects the loss of material and the rounding of the particles but also indicates that abrasion is random in nature, which is attributed to local variations in angularity, solidity, and mineral composition along the surface of granite particles. Softer minerals such as biotite (mica) and amphibole appear to abrade more easily during the early stages of tumbling, as suggested by the colour of the fines generated, while harder minerals such as feldspar and quartz wear down more gradually as tumbling progresses.

Abrasion can be quantified by the change in the weight of individual particles with tumbling time. In Fig. 10, the weight loss is normalised by the initial weight and plotted against time. In both types of tests, "with grit" and "without grit", the weight decreases steadily, reflecting the cumulative effect of repeated impacts and sustained particle contact. As might be expected, more weight is lost when grit is present, almost 75% of the original weight, compared with about 50% in the absence of grit. Nearly half of the total weight loss seems to occur in the initial stages for both conditions (i.e. within the first 5 days in a 20-day experiment). The substantial and rapid material loss in the with-grit case may indicate that the higher hardness of the grit relative to the granite enhances the abrasive effects. A sharp increase in weight loss occurs at the start of stage 2 in the with-grit case, corresponding to the introduction of medium-sized grit, probably owing to an increase in the number density of grit contacts, whereas the without-grit condition exhibits a smoother, gradually decreasing abrasion rate. Beyond this point, there is no significant change in the rate of weight loss in the with-grit condition as tumbling progresses from stage 2 to stage 4. Weight loss continues throughout the tumbling period and does not fully level off, in line with the observations of Kuenen [28], who reported that in tumbling, pebbles lost most of their weight early on, with the rate of loss tapering off over time. The presence of grit in multiparticle tumbling keeps the scatter in abrasion response low in comparison to without grit, as shown by the error bars in Fig. 10. At each tumbling interval, images were obtained for both the with-grit and the without-grit conditions. These images were processed in MATLAB to derive the shape parameters and descriptors discussed in the subsequent sections. A detailed description of the methodology is provided in Section S.1 of the Supplementary document.

The significant morphological changes include changes in particle size and in particle shape (e.g. roundness). In tests both with and without grit, the equivalent particle diameter decreases, with a significant decrease during the initial stages of tumbling, as shown by the probability density functions of the particle size in Fig. 11. Over the 20-day (28,800 min) duration of the tests, the particle size distributions converge towards a narrow size range of approximately 16 to 24 mm for the with-grit condition (Fig. 11a) and 20 to 32 mm for the without-grit condition (Fig. 11b), as indicated by the tightly clustered red and orange curves, although the process is slower when no grit is present. The wear mechanisms can also be inferred: the with-grit curves exhibit a well-defined peak that shifts smoothly towards smaller sizes with time,

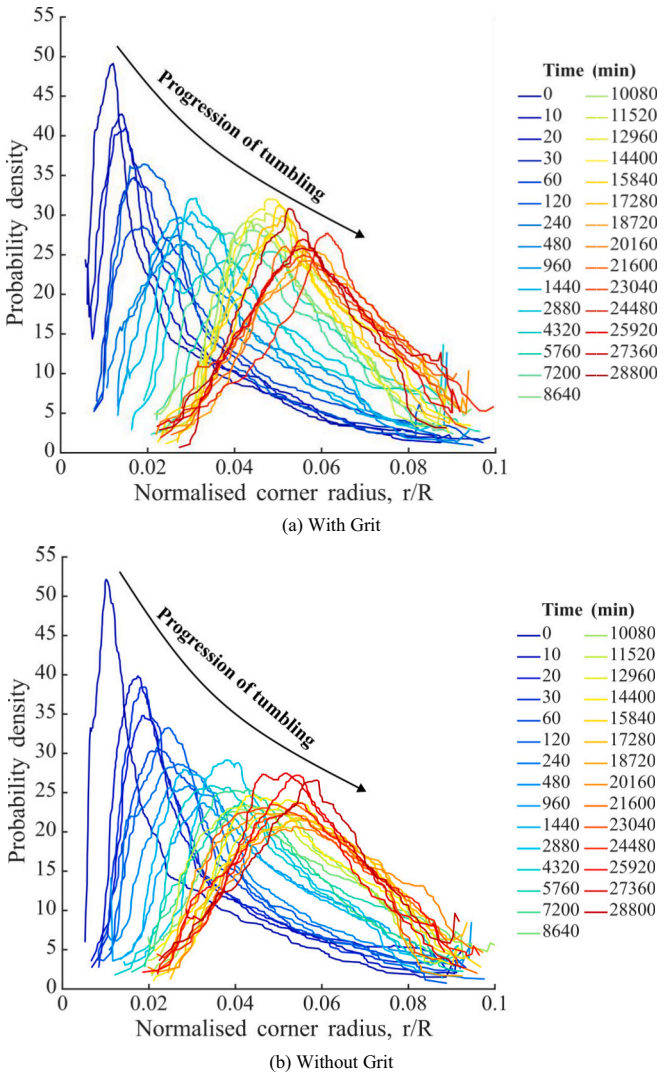


Fig. 12. Effect of progressive multiparticle tumbling on particle corner radius: (a) With grit, (b) Without grit.

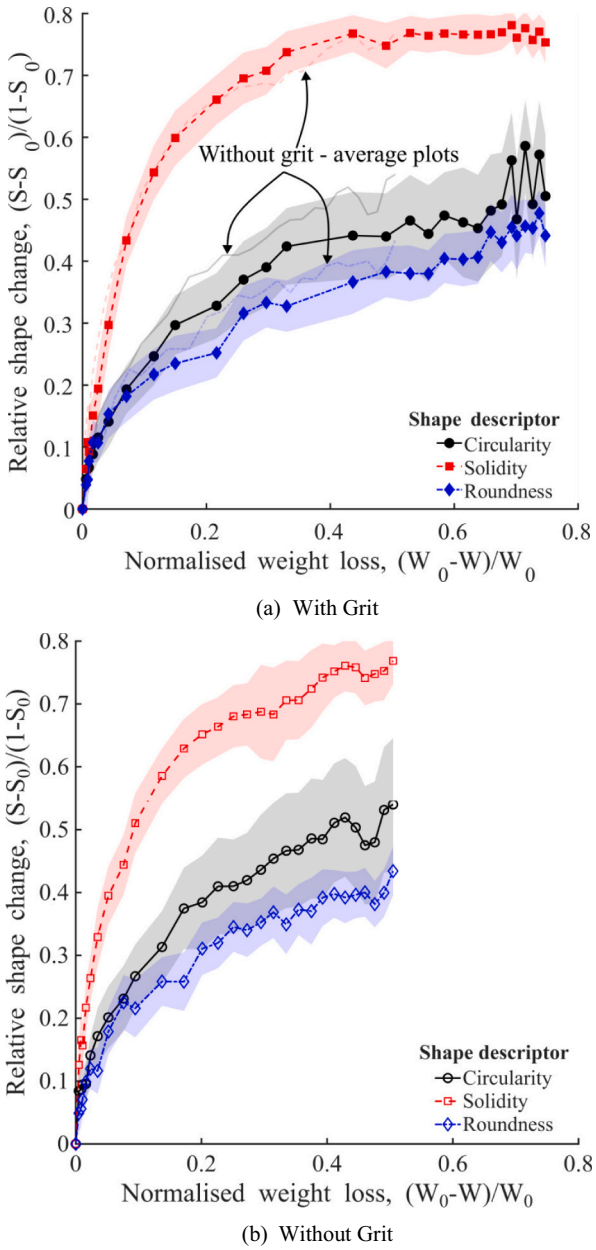


Fig. 13. Evolution of average particle shape descriptors with progressive weight loss in multiparticle tumbling: (a) With grit, (b) Without grit. The shaded region represents the 95% confidence interval of the mean, $n = 30$ particles.

indicative of uniform, steady-state surface abrasion across the population, whereas the without-grit distributions remain broader and flatter, reflecting heterogeneous size reduction and variable abrasion rates among individual particles.

Normalising the corner radius r (i.e. the radius of curvature at a particle's corners) by the radius R of the largest inscribed circle of the particle provides a measure of rounding that is distinct from the overall sphericity (Fig. 12) but recalls the roundness parameter proposed by Wadell [46]. Also plotted as probability density functions, the distributions shift to the right with time, indicating progressive rounding. Initially, both conditions have sharp peaks corresponding to a normalised corner radius of around 0.01. By the final stage, the with-grit sample peaks at around 0.06 with a broader distribution (Fig. 12a), while the without-grit sample peaks near 0.05 with a narrower distribution (Fig. 12b).

Fig. 13 shows how the particle shape descriptors, namely circularity (the ratio of the perimeter of an equivalent circle with the same area as the particle to the perimeter of the particle), solidity (the ratio of the actual particle area to the convex hull area), and roundness (the ratio of average corner radius to radius of inscribed circle) evolve with progressive weight loss. In Fig. 13a and b, the shaded regions show the scatter of shape evolution for the data from all particles with the progression of tumbling with grit and without grit, respectively. As seen with the weight loss, a rapid change occurs during the early stages of tumbling. This reflects significant morphological modifications, consistent with the changes in particle boundary observed in Fig. 9. The changes then become more gradual as the material is progressively abraded and the values of the shape descriptors approach unity. This

Table 3
Average shape descriptors over all thirty particles for tumbling with and without grit.

Time (days)	Grit			Without grit		
	Circularity	Solidity	Roundness	Circularity	Solidity	Roundness
0	0.818 ± 0.053	0.967 ± 0.012	0.270 ± 0.072	0.821 ± 0.068	0.968 ± 0.013	0.285 ± 0.076
20	0.902 ± 0.083	0.993 ± 0.003	0.598 ± 0.085	0.911 ± 0.072	0.993 ± 0.004	0.598 ± 0.073

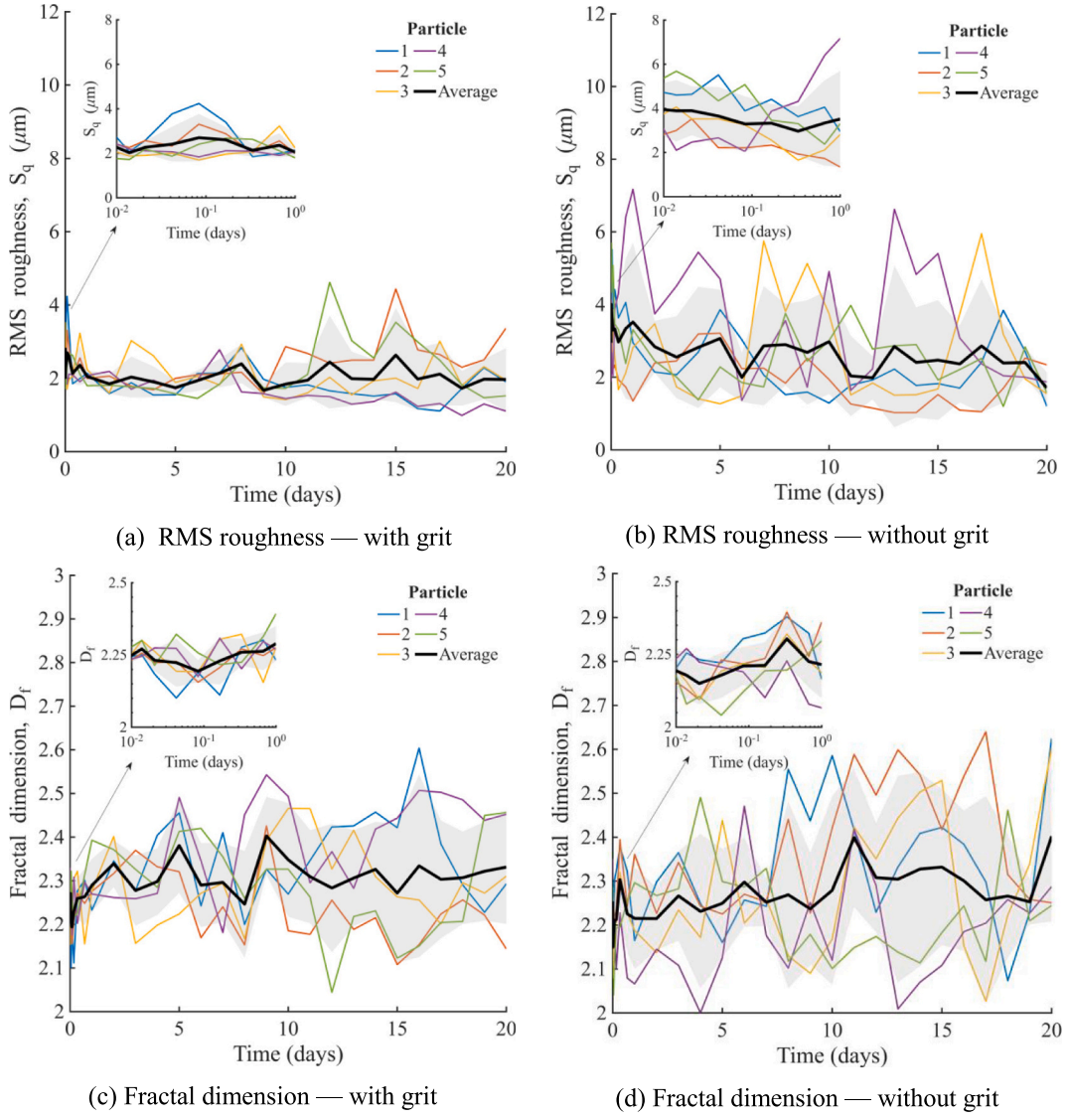


Fig. 14. Evolution of particle roughness and fractal dimension with progressive weight loss in multiparticle tumbling: (a) RMS roughness — with grit, (b) RMS roughness — without grit, (c) Fractal dimension — with grit, (d) Fractal dimension — without grit. The shaded region represents ±1 standard deviation ($n = 5$ particles).

behaviour reflects the fact that once particles become more rounded, the rate of abrasion decreases and only minor changes in overall shape occur. This agrees with the observations of Kuenen [28] and Khanal and Morrison [47], who reported that particles with higher roundness lose less mass per unit time or rolling distance, and with the finding that, as shapes become more regular, they become more resistant to further abrasion [48].

The initial and final values of the shape descriptors for tumbling with and without grit are presented in Table 3. Interestingly, although the shape descriptors change more rapidly with weight loss in the presence of grit, their final values are broadly similar in the two conditions.

To obtain a complete picture of particle evolution in multiparticle

tumbling, the surface roughness of five particles from each tumbling condition was analysed. The particles were scanned at successive time intervals at approximately the same location to monitor the evolution of their surface characteristics throughout the process. To quantify these changes, two primary metrics were considered: the root-mean-square roughness and the fractal dimension.

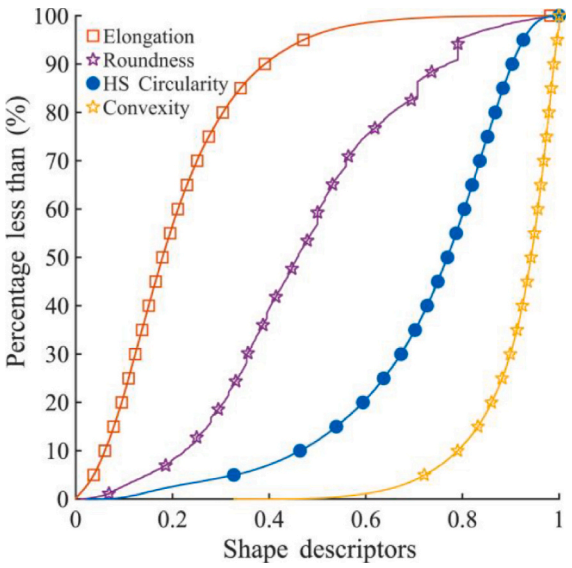
Fig. 14a and b present the root-mean-square roughness values for the five particles over the full duration of tumbling for both the with-grit and without-grit conditions, with inset plots highlighting the very early stages of tumbling in minutes. The shaded regions show the scatter in the rms roughness and fractal dimension. These figures show no clear relationship between root-mean-square roughness and tumbling time, in contrast to the behaviour of the other parameters and shape descriptors, because there is significant scatter in the roughness values at all stages of tumbling. This behaviour is further seen in Fig. 14c and d, which show the evolution of the fractal dimension with tumbling time. As with the root-mean-square roughness, no consistent trend is observed in the fractal dimension. Instead, substantial variability and randomness are present.

However, a clear distinction exists between the two tumbling conditions. Examination of Fig. 14a and c indicates that the with-grit condition produces more uniform curves, with less variability in root-mean-square roughness than the without-grit condition, in which the data are more dispersed and highly erratic. This suggests that surface roughness evolution is more controlled in the presence of grit. In the early stages of tumbling, the root-mean-square roughness under the with-grit condition ranges from approximately 2 to 4 μm and remains within a similar range in later stages as the curves converge. In contrast, the without-grit condition exhibits a wider spread of values, ranging from approximately 3.5 to 6 μm in the early stages and from 3 to 6.5 μm in later stages. Similarly, for the fractal dimension, values under the with-grit condition range from approximately 2.1 to 2.3 in the early stages of tumbling and remain within a comparable range in later stages, as the curves converge. The without-grit condition, on the other hand, shows a much greater degree of scatter, with values spanning roughly 2.01 to 2.23 initially and broadening further to between 2.0 and 2.6 as tumbling continues.

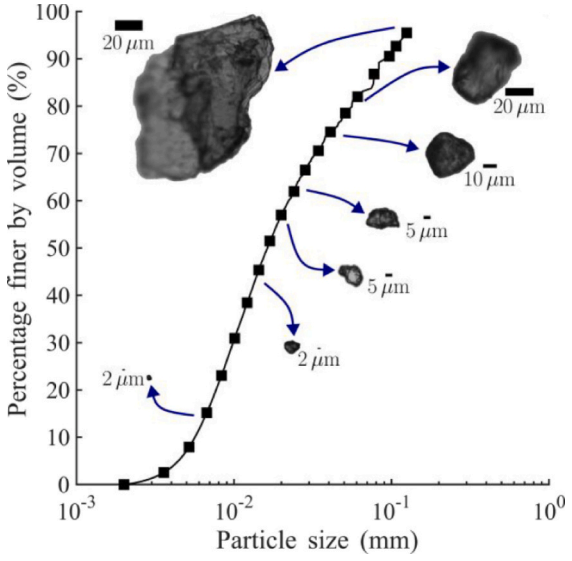
Although the polish grit in the with-grit condition would be expected to produce smoother surfaces, significant scatter is observed, similar to that in the without-grit condition, because repeated impacts between particles during tumbling prevent a uniform reduction in surface roughness at the microscale.

The collective randomness observed in both surface roughness and fractal dimension suggests that multiparticle tumbling, although perhaps more representative of natural weathering, is an ineffective method for achieving controlled changes in surface texture. Given the exploratory nature of this study, measuring the surface roughness of 5 out of 30 particles for each tumbling condition may not be sufficient for statistical significance, and further studies should consider a larger number of particles. Precision in roughness modification is best achieved through controlled single-particle tumbling, as shown in Fig. 7, where the process is dominated by particle–grit interaction rather than by the complex particle–grit–particle interactions in multiparticle tumbling shown in Fig. 14. Consequently, multiparticle tumbling is most effective when the objective is the modification of overall particle morphology and shape. Single particle tumbling in the presence of grit and multiparticle tumbling for granite particles can facilitate demarcation of the effect of roughness and shape on micro- and macro-scale stiffness and strength behaviour.

Analysis of the residual fines generated during tumbling shows that



(a) Shape distribution by count



(b) Size distribution by volume

Fig. 15. Shape and size distribution of residue particles in multiparticle tumbling: (a) Shape distribution by count, (b) Size distribution by volume.

their particle shape is not uniform and varies with the descriptor considered (Fig. 15a). Analysis of their particle size distribution (cumulative volume-based particle size distribution in Fig. 15b) shows a smooth S-shaped trend, nearly fractal for sizes above 20 μm, covering a broad size range of approximately 2–100 μm, with the majority of the particle volume concentrated between 10 and 30 μm. Scanned images of particles in the different size ranges are shown alongside the particle size distribution. The finer particles, particularly at about 2 and 5 μm, appear more regular and sub-rounded, whereas particles in the coarser fraction above 50 μm show greater angularity, more irregular outlines, and sharper edges. Whereas the coarser, angular residue particles may represent "freshly chipped" asperities, the finer ones may be the product of further degradation of those chipped-off asperities during tumbling.

6. Conclusions

This study investigated the evolution of the surface of granite ballast particles during rotary tumbling in the presence or absence of abrasive grit. Single-particle tumbling with hard grit was performed to isolate and examine changes in surface roughness during the tumbling process, as this is the primary mechanism of change, with little to no variation in particle size or overall shape. Multiparticle tumbling with and without grit was mainly used to study changes in particle size and shape, which are the dominant effects in this case, whereas changes in surface roughness are secondary and sporadic and cannot be isolated and investigated. Analysis of the morphology of the tested particles, from the mesoscale (size and shape) to the microscale (surface roughness), together with the abrasion rate, highlighted a potential new method of creating granite ballast particles with controlled morphology.

In single-particle tumbling, the interaction of a hemispherical granite particle with abrasive grit was studied. Four types of grit (made of silicon carbide and aluminium oxide) were used sequentially in four stages. Grit morphology was studied to characterise the effect of the abrasive grit on the ballast particles. The surface of a hemispherical ballast particle was examined through optical images and surface height maps. In the initial stages, the coarse silicon carbide grit caused surface brightening and the removal of large asperities, which appears to be associated with the removal of biotite (mica). In the intermediate stages, the removal of amphibole appears to have contributed to the formation of small crater-like features on the particle surface, while the number of small asperities increased significantly. With polish grit in the later stages, quartz and feldspar became progressively polished, exhibiting a glassy appearance and low surface roughness.

In multiparticle tumbling, granite ballast particles collide with one another, modifying their surfaces through attrition, chipping, and rounding. The particle weight loss with time was consistent with observations reported in earlier studies (e.g. Kuenen [28]). Examination of particle boundaries with time suggested that the angular and non-convex parts of the boundaries undergo more wear than the convex and rounded parts. However, this non-uniform abrasion did not strongly influence the final particle shape after 20 days of tumbling, as the particles still carried the signature of their initial shapes. The size of the ballast particles decreased progressively with time, and the presence of abrasive grit accelerated the wear process. The corners of particles also became more rounded with time; however, they could still easily be identified as corners even after 20 days of tumbling. Shape descriptors, including circularity, roundness, and solidity, exhibited significant changes during the early stages of tumbling, followed by stabilisation in later stages, with solidity increasing more rapidly than the others. Changes in these parameters were also linked to particle weight loss, since significant shape modification requires substantial weight loss; minimal variation was observed once the particles became well rounded. The roughness of the ballast particles, as assessed by S_q and D_f, showed no consistent trend; however, the presence of abrasive grit reduced the scatter in both parameters. The fines generated during multiparticle tumbling were also analysed in terms of size and shape. The particle size distribution was nearly fractal, indicating a self-similar pattern across multiple scales.

Mechanical tumbling is an effective method for controlling surface roughness and texture, and is widely applied in fields where surface characteristics are critical. Despite its broad use, further investigation is required to better understand the governing mechanisms, particularly across different granular materials, as the present study focuses only on UK granite.

CRediT authorship contribution statement

Emmanuel Okebunor Ashinze: Writing – review & editing, Writing – original draft, Software, Methodology, Investigation, Formal analysis, Data curation, Conceptualization. **Saurabh Singh:** Writing – review & editing, Writing – original draft, Visualization, Software, Methodology, Investigation, Formal analysis, Conceptualization. **Matthew Richard Coop:** Writing – review & editing, Supervision, Resources, Project administration, Methodology, Investigation, Funding acquisition, Conceptualization. **Beatrice Anne Baudet:** Writing – review & editing, Supervision, Resources, Project administration, Methodology, Investigation, Funding acquisition.

Declaration of competing interest

The authors declare that they have no known competing financial interests or personal relationships that could have appeared to influence the work reported in this paper.

Acknowledgements

The authors are grateful for the technical support provided by Mr. Charlie Laybourn-Waller. SS also acknowledges Ms. Man Li for providing access to computational resources during part of this study. The work was funded by the Engineering and Physical Sciences Research Council (EPSRC) through grants EP/W000563/1, EP/T517793/1, and EP/W524335/1.

Appendix A. Repeatability test for roughness (Keyence microscope)

To assess the reliability of the surface measurements made with the Keyence microscope, a repeatability test was conducted. Although several particles were scanned, the results presented here focus on a hemispherical granite particle as a representative sample; similar trends were observed across all samples. The particle was scanned over approximately the same area five times. After each scan, it was removed and repositioned on the microscope to assess the consistency of the scan outputs and the variation in measurements. The peak height distribution, shown in Fig. A.1.a, was used to assess the reliability of the microscope. Peak heights and their counts were plotted with error bars representing the five scans, and the plots show that the scans produced highly consistent counts, indicating reliable measurements. In addition, power-spectral-density analysis was carried out for these repeatability scans. The PSD is quite uniform for these five scans (Fig. A.1.b), and rms roughness, slope, and curvature also remain nearly constant (Fig. A.1.c). This demonstrates the repeatability of scans (without modifying the surface) for both peak-count and power-spectral density analysis.

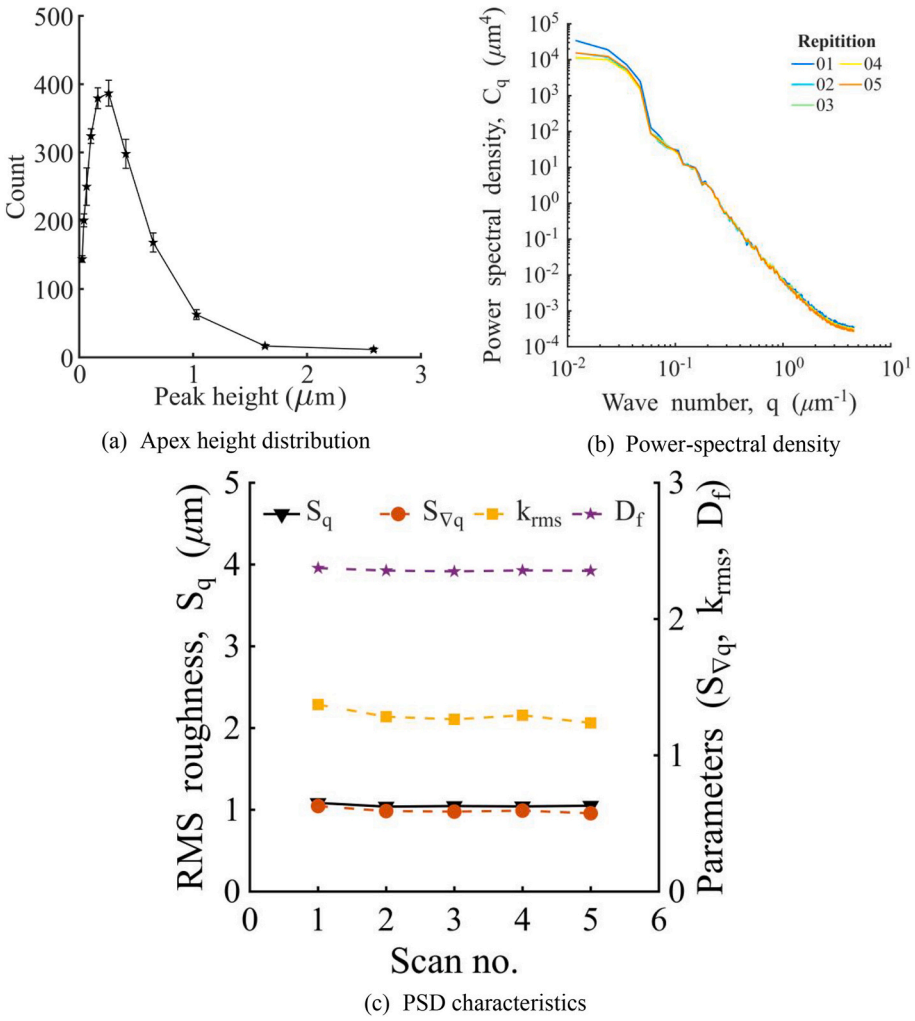
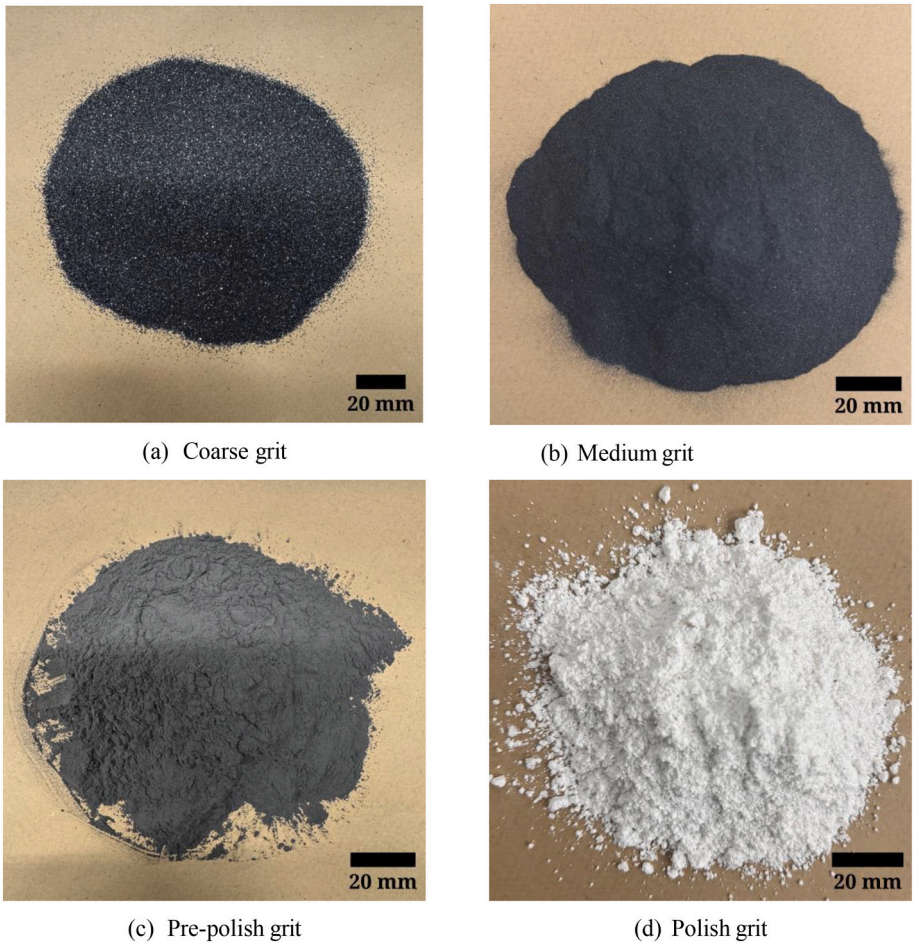


Fig. A.1. Repeatability test for roughness measurement of hemispherical granite ballast: (a) Apex height distribution, (b) Power-spectral density, (c) PSD characteristics.

Appendix B. Powder grits

The abrasive powders (grits) employed across the four tumbling stages comprised silicon carbide and aluminium oxide. Silicon carbide was used in the first three stages, while aluminium oxide was applied in the final stage. Heaps of the abrasive powders are shown in Fig. B.1.



(a) Coarse grit (b) Medium grit

(c) Pre-polish grit (d) Polish grit

Fig. B.1. Images of powder grits.

Appendix C. Supplementary data

The supplementary document presents the raw images of the particles at successive tumbling intervals, together with a detailed description of the shape-analysis method used to obtain the various shape parameters for multiparticle tumbling in this study. It also reports how other parameters, such as particle dimensions, evolved with time and how they relate to weight loss. As with the single-particle tumbling, the peak height count and mean height distribution for the multiparticle tumbling are also presented. Supplementary data to this article can be found online at [https://doi.org/10.1016/j.powtec.2026.123416].

Data availability

Data is provided in supplementary document in raw form and in the manuscript as processed figures.

References

[1] P.H. Kuenen, Sand, Sci. Am. 202 (4) (1960) 94–113.
[2] A.J. Moss, Origin, shaping and significance of quartz sand grains, J. Geol. Soc. Aust. 13 (1) (1966) 97–136, https://doi.org/10.1080/00167616608728607.
[3] D.H. Krinsley, I.J. Smalley, Sand: the study of quartz sand in sediments provides much information about ancient geological environments, Am. Sci. 60 (3) (1972) 286–291.
[4] M. Meybeck, Global chemical weathering of surficial rocks estimated from river dissolved loads, Am. J. Sci. 287 (5) (1987) 401–428, https://doi.org/10.2475/ajs.287.5.401.
[5] T.W. Lambe, R.V. Whitman, Soil Mechanics, SI Version, John Wiley & Sons, 2008.
[6] A. Saeed, J.W. Hall, W. Barker, Performance-Related Tests of Aggregates for Use in Unbound Pavement Layers, NCHRP Report 453, Transportation Research Board, National Research Council, Washington, DC, 2001.
[7] S. Bodek, D.J. Jerolmack, Breaking down chipping and fragmentation in sediment transport: the control of material strength, Earth Surf. Dyn. 9 (6) (2021) 1531–1543, https://doi.org/10.5194/esurf-9-1531-2021.
[8] B. Indraratna, W. Salim, C. Rujikiatkamjorn, Advanced Rail Geotechnology: Ballasted Track, Second ed., CRC Press, Boca Raton, 2023 https://doi.org/10.1201/9781003278979.
[9] C.A. Bareither, T.B. Edil, C.H. Benson, D.M. Mickelson, Geological and physical factors affecting the friction angle of compacted sands, J. Geotech. Geoenviron. Eng. 134 (10) (2008) 1476–1489, https://doi.org/10.1061/(ASCE)1090-0241(2008)134:10(1476).
[10] I. Cavarretta, M. Coop, C. O'Sullivan, The influence of particle characteristics on the behaviour of coarse grained soils, Géotechnique 60 (6) (2010) 413–423, https://doi.org/10.1680/geot.2010.60.6.413.
[11] J. Yang, X.Q. Gu, Shear stiffness of granular material at small strains: does it depend on grain size? Géotechnique 63 (2) (2013) 165–179, https://doi.org/10.1680/geot.11.P.083.
[12] J. Yang, X.D. Luo, Exploring the relationship between critical state and particle shape for granular materials, J. Mech. Phys. Solids 84 (2015) 196–213, https://doi.org/10.1016/j.jmps.2015.08.001.
[13] F.N. Altuhafi, M.R. Coop, V.N. Georgiannou, Effect of particle shape on the mechanical behavior of natural sands, J. Geotech. Geoenviron. Eng. 142 (12) (2016) 04016071, https://doi.org/10.1061/(ASCE)GT.1943-5606.0001569.
[14] K.A. Murphy, A.K. MacKeith, L.K. Roth, H.M. Jaeger, The intertwined roles of particle shape and surface roughness in controlling the shear strength of a granular

material, Granul. Matter 21 (3) (2019) 72, https://doi.org/10.1007/s10035-019-0913-7.
[15] H. Hertz, Ueber die Berührung fester elastischer Körper, J. Reine Angew. Math. 92 (1882) 156–171, https://doi.org/10.1515/crll.1882.92.156.
[16] J.A. Greenwood, J.H. Tripp, The elastic contact of rough spheres, J. Appl. Mech. 34 (1) (1967) 153–159, https://doi.org/10.1115/1.3607616.
[17] K.L. Johnson, J.A. Greenwood, J.G. Higginson, The contact of elastic regular wavy surfaces, Int. J. Mech. Sci. 27 (6) (1985) 383–396, https://doi.org/10.1016/0020-7403(85)90029-3.
[18] B.N.J. Persson, Theory of rubber friction and contact mechanics, J. Chem. Phys. 115 (8) (2001) 3840–3861, https://doi.org/10.1063/1.1388626.
[19] J. Harkness, A. Zervos, L. Le Pen, S. Aingaran, W. Powrie, Discrete element simulation of railway ballast: modelling cell pressure effects in triaxial tests, Granul. Matter 18 (3) (2016) 65, https://doi.org/10.1007/s10035-016-0660-y.
[20] M. Tolomeo, G.R. McDowell, Implementation of real contact behaviour in the DEM modelling of triaxial tests on railway ballast, Powder Technol. 412 (2022) 118021, https://doi.org/10.1016/j.powtec.2022.118021.
[21] M. Otsubo, C. O'Sullivan, Experimental and DEM assessment of the stress-dependency of surface roughness effects on shear modulus, Soils Found. 58 (3) (2018) 602–614, https://doi.org/10.1016/j.sandf.2018.02.020.
[22] F. Altuhafi, B.A. Baudet, M.R. Coop, An investigation of the applicability of contact models to the normal load-deformation behaviour of artificially shaped granite, Acta Geotech. 19 (6) (2024) 3447–3465, https://doi.org/10.1007/s11440-023-02123-9.
[23] S. Utermann, P. Aurin, M. Benderoth, C. Fischer, M. Schröter, Tailoring the frictional properties of granular media, Phys. Rev. E 84 (3) (2011) 031306, https://doi.org/10.1103/PhysRevE.84.031306.
[24] F. Ning, D. Zou, G. Cui, J. Liu, D. Li, Y. Fu, The effect of particle shape on particle breakage and shape evolution in gravelly soils, Transp. Geotech. 51 (2025) 101538, https://doi.org/10.1016/j.trgeo.2025.101538.
[25] R.P. Trotta, E.V. Barroso, L.M.G. da Motta, Migmatitic gneiss aggregates: compositional, mechanical, and morphological responses to innate heterogeneity, Eng. Geol. 283 (2021) 106002, https://doi.org/10.1016/j.enggeo.2021.106002.
[26] C.K. Wentworth, A laboratory and field study of cobble abrasion, J. Geol. 27 (7) (1919) 507–521, https://doi.org/10.1086/622676.
[27] W.C. Krumbein, The effects of abrasion on the size, shape and roundness of rock fragments, J. Geol. 49 (5) (1941) 482–520, https://doi.org/10.1086/624985.
[28] P.H. Kuenen, Experimental abrasion of pebbles: 2. Rolling by current, J. Geol. 64 (4) (1956) 336–368, https://doi.org/10.1086/626370.
[29] P.W. Cleary, R.D. Morrison, Comminution mechanisms, particle shape evolution and collision energy partitioning in tumbling mills, Miner. Eng. 86 (2016) 75–95, https://doi.org/10.1016/j.mineng.2015.12.006.
[30] I. Deiros Quintanilla, G. Combe, F. Emeriault, C. Voivret, J.F. Ferellec, X-ray CT analysis of the evolution of ballast grain morphology along a Micro-Deval test: key role of the asperity scale, Granul. Matter 21 (2) (2019) 30, https://doi.org/10.1007/s10035-019-0881-y.
[31] A. Paixão, E. Fortunato, Abrasion evolution of steel furnace slag aggregate for railway ballast: 3D morphology analysis of scanned particles by close-range photogrammetry, Constr. Build. Mater. 267 (2021) 121225, https://doi.org/10.1016/j.conbuildmat.2020.121225.
[32] T. Yao, H. Yang, S.D. Lourenço, B.A. Baudet, F.C. Kwok, Multi-scale particle morphology evolution in rotating drum tests: Role of particle shape and pore fluid, Eng. Geol. 303 (2022) 106669, https://doi.org/10.1016/j.enggeo.2022.106669.
[33] A. Afrouz, Practical Handbook of Rock Mass Classification Systems and Modes of Ground Failure, CRC Press, Boca Raton, 1992.
[34] P.W. Scott, G.K. Rollinson, Crushed rock aggregates: their mineralogy and textures using automated scanning electron microscopy, in: E. Hunger, T.J. Brown (Eds.), Proceedings of the 18th Extractive Industry Geology Conference, EIG Conferences, 2015, pp. 49–68.
[35] N. Domede, T. Parent, A. Sellier, Mechanical behaviour of granite: a compilation, analysis and correlation of data from around the world, Eur. J. Environ. Civ. Eng. 23 (2) (2019) 193–211, https://doi.org/10.1080/19648189.2016.1275984.
[36] A. Nastic, A. Merati, M. Bielawski, M. Bolduc, O. Fakolujo, M. Nganbe, Instrumented and Vickers indentation for the characterization of stiffness, hardness and toughness of zirconia-toughened Al_2O_3 and SiC armor, J. Mater. Sci. Technol. 31 (8) (2015) 773–783, https://doi.org/10.1016/j.jmst.2015.06.005.
[37] A. Krell, S. Schädlich, Nanoindentation hardness of submicrometer alumina ceramics, Mater. Sci. Eng. A 307 (1–2) (2001) 172–181, https://doi.org/10.1016/S0921-5093(00)01818-9.
[38] F.N. Altuhafi, M.R. Coop, The effect of mode of loading on particle-scale damage, Soils Found. 51 (5) (2011) 849–856, https://doi.org/10.3208/sandf.51.849.
[39] J. Zheng, R.D. Hryciw, Traditional soil particle sphericity, roundness and surface roughness by computational geometry, Géotechnique 65 (6) (2015) 494–506, https://doi.org/10.1680/geot.14.P.192.
[40] P.R. Nayak, Random process model of rough surfaces, J. Lubr. Technol. 93 (3) (1971) 398–407, https://doi.org/10.1115/1.3451608.
[41] H. Yang, B.A. Baudet, T. Yao, Characterization of the surface roughness of sand particles using an advanced fractal approach, Proc. R. Soc. A 472 (2194) (2016) 20160524, https://doi.org/10.1098/rspa.2016.0524.
[42] C. Mo, J. Zhao, D. Zhang, Real-time measurement of mechanical behavior of granite during heating-cooling cycle: a mineralogical perspective, Rock Mech. Rock Eng. 55 (7) (2022) 4403–4422, https://doi.org/10.1007/s00603-022-02867-y.
[43] M. Otsubo, C. O'Sullivan, W.W. Sim, E. Ibraim, Quantitative assessment of the influence of surface roughness on soil stiffness, Géotechnique 65 (8) (2015) 694–700, https://doi.org/10.1680/geot.14.T.028.
[44] B.N.J. Persson, O. Albohr, U. Tartaglino, A.I. Volokitin, E. Tosatti, On the nature of surface roughness with application to contact mechanics, sealing, rubber friction and adhesion, J. Phys.: Condens. Matter 17 (1) (2005) R1–R62, https://doi.org/10.1088/0953-8984/17/1/R01.
[45] M. Khanal, R. Morrison, Discrete element method study of abrasion, Miner. Eng. 21 (11) (2008) 751–760, https://doi.org/10.1016/j.mineng.2008.06.008.
[46] H. Wadell, Volume, shape, and roundness of rock particles, J. Geol. 40 (5) (1932) 443–451, https://doi.org/10.1086/623964.
[47] M. Khanal, R. Morrison, DEM simulation of abrasion of nonspherical particles in tumbling mill, Part. Sci. Technol. 27 (1) (2009) 68–76, https://doi.org/10.1080/02726350802611853.
[48] T. Szabó, G. Domokos, J.P. Grotzinger, D.J. Jerolmack, Reconstructing the transport history of pebbles on Mars, Nat. Commun. 6 (1) (2015) 8366, https://doi.org/10.1038/ncomms9366.